

dient from $z = D_0$ to $z = \infty$ yields $F_{\text{tip-sample}} = -0.14 \text{ nN}$ (attractive) as the force acting between tip and sample when the PL is closest to the surface.

REFERENCES AND NOTES

1. G. Binnig, H. Rohrer, Ch. Gerber, E. Weibel, *Phys. Rev. Lett.* **50**, 120 (1983).
2. G. Binnig, C. F. Quate, Ch. Gerber, *ibid.* **56**, 930 (1986).
3. G. Meyer and N. M. Amer, *Appl. Phys. Lett.* **56**, 2100 (1990).
4. F. Ohnesorge and G. Binnig, *Science* **260**, 1451 (1993).
5. These tips are called Ultralevers (Park Scientific Instruments, Sunnyvale, CA).
6. F. J. Giessibl and G. Binnig, *Ultramicroscopy* **42**, 281 (1992).
7. L. Howald, R. Luethi, E. Meyer, P. Guethner, H.-J. Guentherodt, *Z. Phys. B* **93**, 267 (1994).
8. F. J. Giessibl, *Jpn. J. Appl. Phys.* **33**, 3726 (1994).
9. AutoProbe VP 900 (Park Scientific Instruments).
10. F. J. Giessibl and B. M. Trafts, *Rev. Sci. Instrum.* **65**, 1923 (1994).
11. M. Tortorese, R. C. Barrett, C. F. Quate, *Appl. Phys. Lett.* **62**, 834 (1993).
12. T. R. Albrecht, P. Grutter, D. Horne, D. Rugar, *J. Appl. Phys.* **69**, 668 (1991).
13. The forces acting between tip and sample during STM operation have been measured by mounting a sample on a CL and monitoring the variation of the oscillation frequency of the sample-CL assembly by fm detection of the tunneling current [U. Dürig, O. Züger, D. W. Pohl, *Phys. Rev. Lett.* **65**, 349 (1990); U. Dürig and O. Züger, *Phys. Rev. B* **50**, 5008 (1994); and references therein].
14. VPPL40NO (Park Scientific Instruments).
15. The dominant low-frequency noise component in fm detection is the variation of the eigenfrequency of the PL with temperature. This frequency shift is very small for appropriate oscillation amplitudes (10) compared with the frequency shift resulting from the tip-sample interaction and can be neglected.
16. The sample was prepared by cleaning a Si(111)-oriented wafer in acetone and alcohol in an ultrasonic

bath for 5 min, transferring it into the vacuum chamber, and then heating it to 1170°C by electron beam heating. The pressure during heating increased to 1.3×10^{-9} mbar. The base pressure of the vacuum system is 5×10^{-11} mbar.

17. K. Takayanagi, Y. Tanishiro, M. Takahashi, S. Takahashi, *J. Vac. Sci. Technol. A* **3**, 1502 (1985).
18. F. J. Giessibl, *Phys. Rev. B* **45**, 13815 (1992).
19. C. Kittel, *Introduction to Solid State Physics* (Wiley, New York, 1986), p. 55.
20. This is a very conservative estimate, because Si is a very brittle material, and the actual range of the attractive interatomic potential will be much shorter. For the purpose of this analysis, this estimate is sufficient because the uncertainty in the tip-sample interaction is much larger.
21. Assuming a tip-sample potential with a constant force gradient Δk , a range λ , and a tip oscillating with an elongation according to $z(t) = D_0 + A_0 - A_0 \cos(2\pi\nu_0 t)$, the effective force constant $k = k_{\text{PL}} + \Delta k$ for $-t^* < t \leq t^*$ and $k = k_{\text{PL}}$ for $t^* < t \leq T - t^*$, with $t^* = [7/(2\pi)] \arccos(1 - \lambda/A_0)$ and $T = 1/\nu_0$. Accordingly, the resulting frequency shift will be smaller than in Eq. 2 for large oscillation amplitudes, namely

$$\frac{\Delta\nu}{\nu_0} \approx \frac{1}{\pi} \arccos\left(1 - \frac{\lambda}{A_0} \frac{\Delta k}{2k_{\text{PL}}}\right)$$

where $\Delta k/k_{\text{PL}} \ll 1$ and $\lambda/A_0 \ll 1$. This can be further simplified [with use of $\cos x \approx 1 - (x^2/2)$ for $x \ll 1$] to

$$\frac{\Delta\nu}{\nu_0} \approx \frac{\sqrt{2}}{\pi} \sqrt{\frac{\lambda}{A_0} \frac{\Delta k}{2k_{\text{PL}}}}$$

22. I thank C. F. Quate for his continuous support, B. M. Trafts for sharing his experience of imaging Si(111)-(7×7) using the STM with me, M. D. Kirk for technical discussions and bringing his enthusiasm to this project, S. Yoshikawa for help with sample preparation, J. Nogami for useful comments, and S. Presley for his technical support. M. Tortorese supplied me with PLs and an understanding of how to use them, and T. R. Albrecht shared his knowledge of fm detection with me.

30 August 1994; accepted 31 October 1994

Atomic-Scale Images of the Growth Surface of $\text{Ca}_{1-x}\text{Sr}_x\text{CuO}_2$ Thin Films

Kazumasa Koguchi, Takuya Matsumoto, Tomoji Kawai*

The surface microstructure of *c*-axis $(\text{Ca,Sr})\text{CuO}_2$ thin films, grown by laser molecular beam epitaxy on $\text{SrTiO}_3(001)$ substrates, was studied by ultrahigh-vacuum scanning tunneling microscopy (STM). Images were obtained for codeposited $\text{Ca}_{1-x}\text{Sr}_x\text{CuO}_2$ thin films, which show a layered-type growth mode. The surfaces consist of atomically flat terraces separated by steps that are one unit cell high. A pronounced dependence of the growth mechanism on the Sr/Ca ratio of the films was observed. Atomic resolution STM images of the CuO_2 sheets in the *ab* plane show a square lattice with an in-plane spacing of 4 angstroms; the lattice contains different concentrations of point defects, depending on the polarity of the sample-tip bias.

Since the parent compound of the cuprate superconductors, $(\text{Ca,Sr})\text{CuO}_2$, was first synthesized by Siegrist *et al.* (1), this material has been studied intensively. The principal reason for this interest is that this

compound has the simplest oxygen defect type perovskite structure comprising the CuO_2 sheets that are considered essential for high- T_c superconductivity (T_c is the superconducting transition temperature). STM has been shown to be a powerful technique for imaging high- T_c cuprates on an atomic scale (2–12). Because of the simple structure of the parent compound,

STM offers the opportunity to directly probe the CuO_2 sheets without the interference of intermediate oxide layers. For the purpose of the STM studies, thin film specimens are especially attractive because they provide a well-defined surface that can be preserved from vacuum-type growth conditions (13). It is also of interest to study the layer-by-layer growth mechanism as reflected in systematic changes in the surface structure.

In this report, we describe thin films of $(\text{Ca,Sr})\text{CuO}_2$ deposited on $\text{SrTiO}_3(001)$ substrates and studied by ultrahigh-vacuum (UHV) STM. We used a combined system for laser molecular beam epitaxy (laser MBE) with reflection high-energy electron diffraction (RHEED) and UHV STM. Film surfaces of codeposited $\text{Ca}_{1-x}\text{Sr}_x\text{CuO}_2$ films with different Sr/Ca ratios were prepared, as well as surfaces containing an extra monolayer of CuO . The STM images of *c*-axis-oriented codeposited $(\text{Ca,Sr})\text{CuO}_2$ films show atomically flat and well-defined terraces. The images provide information about the atomic layer epitaxy of $(\text{Ca,Sr})\text{CuO}_2$ films. These atomic-scale images show square lattices with periods that correspond to the *a*-axis lattice constant.

The $(\text{Ca,Sr})\text{CuO}_2$ thin films were prepared by laser MBE (14) with an ArF excimer laser operating at 193 nm and a repetition rate of 2 to 5 Hz. Targets for the ablation were sintered disks of $\text{Ca}_{1-x}\text{Sr}_x\text{CuO}_2$ ($x = 0.30, 0.55, 0.70$), CuO , and metallic Sr. The ablated species were deposited on 0.01% Nb-doped $\text{SrTiO}_3(001)$ single crystal substrates heated to 500°C. During deposition, NO_2 gas was directed onto the substrate as an oxidizing agent for the growth of the parent compound. The background pressure during growth was 1.0×10^{-5} torr. Before the deposition, the substrate was heated to 600°C under NO_2 gas flow at 1.0×10^{-5} torr for 30 min. Then the substrate temperature was reduced to 500°C, and a monolayer of SrO was deposited to stabilize the initial stages of growth (15, 16). The deposition of a single monolayer of SrO was inferred from the observation of a single RHEED intensity oscillation. During and after the deposition of the film, we repeatedly annealed the sample by interrupting the deposition for about 10 to 20 min to enhance surface migration. After the deposition of several layers of $(\text{Ca,Sr})\text{CuO}_2$, the sample was cooled in NO_2 gas flow. Then gas flow was stopped, and the sample was transferred into the UHV STM chamber with a base pressure of less than 10^{-10} torr. To obtain information about the surface microstructure during atomic layer-by-layer growth, in some experiments we deposited a monolayer of

Institute of Scientific and Industrial Research, Osaka University, Mihogaoka, Ibaraki, Osaka 567, Japan.

*To whom correspondence should be addressed.

CuO on the surface of $\text{Ca}_{0.70}\text{Sr}_{0.30}\text{CuO}_2$ under conditions identical to those described above.

A constant-current STM image was taken of the surface of a *c*-axis-oriented $\text{Ca}_{0.70}\text{Sr}_{0.30}\text{CuO}_2$ thin film on $\text{SrTiO}_3(001)$ (Fig. 1A). Atomically flat terraces and steps are clearly observed. The cross-sectional profile (Fig. 1B) shows that the vertical step height between the terraces is about 3.4 Å, which corresponds well with the *c*-axis unit cell height of $\text{Ca}_{0.70}\text{Sr}_{0.30}\text{CuO}_2$. These results indicate a terrace-like growth mode with vertical growth units of one unit cell during the codeposition of $(\text{Ca,Sr})\text{CuO}_2$. The corresponding RHEED pattern of this film is shown in Fig. 1C. The direction of the incident electron beam is parallel to the $\text{SrTiO}_3[100]$ azimuth. The period of the streaks is about 3.9 Å, which corresponds to the *a*-axis lattice constant of $\text{Ca}_{0.70}\text{Sr}_{0.30}\text{CuO}_2$. The RHEED pattern is streaky, and the electron-transmitted pattern is faint. This pattern indicates that the film has a flat surface with low step density that corresponds well with the STM observations.

Images were also obtained for the surface of a $\text{Ca}_{0.70}\text{Sr}_{0.30}\text{CuO}_2$ film containing an extra CuO monolayer (Fig. 2A). Some particles are observed on the surface, apparently consisting of CuO. The particles were practically absent on the surface of the $\text{Ca}_{0.70}\text{Sr}_{0.30}\text{CuO}_2$ film (see Fig. 1A). An additional terrace step height of 2.1 Å was observed, which does not correspond to the unit cell step height (Fig. 2B). This observation suggests the formation of a molecular CuO overlayer. In the RHEED pattern of this film (Fig. 2C), extra streaks appeared with an in-plane period of 2.6 Å (17) in addition to principal streaks as shown in Fig. 1C. Although small particles were observed by STM, the corresponding RHEED pattern did not contain spots. A comparison between Figs. 1 and 2 suggests that the extra streaks after CuO deposition (17) are related to the 2.1 Å extra steps on the film surface.

The surface structures of $\text{Ca}_{1-x}\text{Sr}_x\text{CuO}_2$ films having different Sr/Ca ratios are shown in Fig. 3. Figure 3A is similar to Fig. 1 and shows that the surface of $\text{Ca}_{0.70}\text{Sr}_{0.30}\text{CuO}_2$ consists predominantly of flat terraces, separated by unit cell-high steps. With increasing Sr concentrations, however, particles are observed on the film surface, most of them located near the terrace step edges. This is illustrated in Fig. 3, B and C, for films having the nominal compositions $\text{Ca}_{0.45}\text{Sr}_{0.55}\text{CuO}_2$ and $\text{Ca}_{0.30}\text{Sr}_{0.70}\text{CuO}_2$, respectively. The mean lateral size of the particles is about 60 Å by 60 Å, and the mean height is about 8 Å.

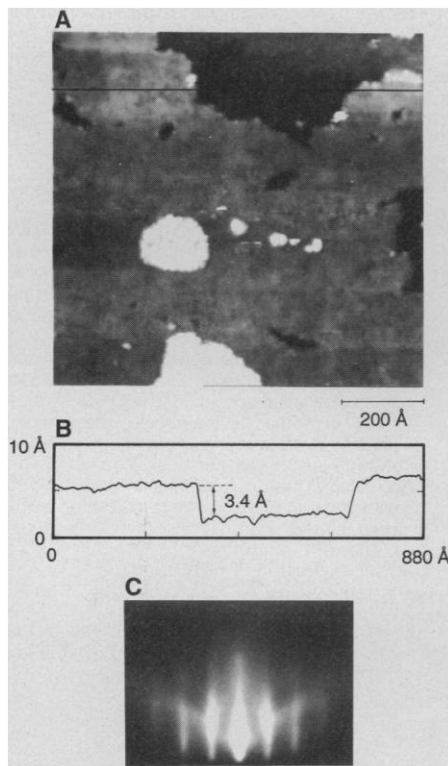


Fig. 1. (A) Constant-current image of a 880 Å by 880 Å region of a $\text{Ca}_{0.70}\text{Sr}_{0.30}\text{CuO}_2$ thin film, taken with a sample bias of 2.0 V and a tunneling current of 0.20 nA. (B) Cross-sectional profile along the line indicated in (A). The difference in vertical height between terraces is about one unit cell height of 3.4 Å. (C) A RHEED pattern of the $\text{Ca}_{0.70}\text{Sr}_{0.30}\text{CuO}_2$ surface. The direction of the incident electron beam is along the $\text{SrTiO}_3[100]$ azimuth.

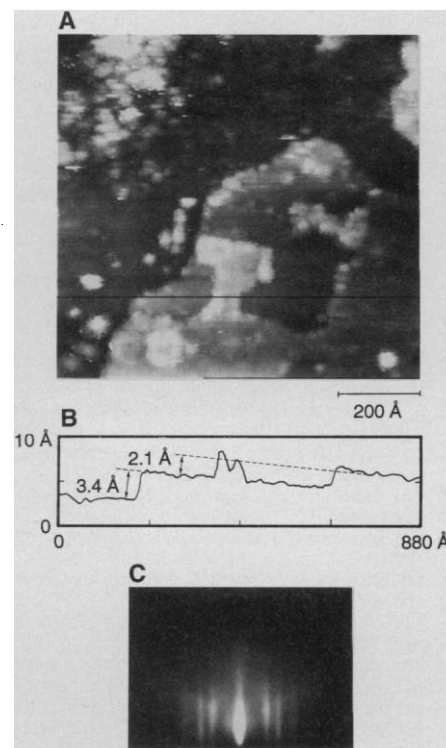


Fig. 2. (A) Constant-current image of a $\text{Ca}_{0.70}\text{Sr}_{0.30}\text{CuO}_2$ surface containing an extra monolayer of CuO. Small particles with a typical lateral size of 50 Å by 50 Å and a vertical height of 8 Å are observed. (B) Cross-sectional profile along the line indicated in (A). Two different step heights of 2.1 and 3.4 Å, respectively, are observed. (C) A RHEED pattern of the CuO-deposited $\text{Ca}_{0.70}\text{Sr}_{0.30}\text{CuO}_2$ surface. The direction of the incident electron beam is along the $\text{SrTiO}_3[100]$ azimuth.

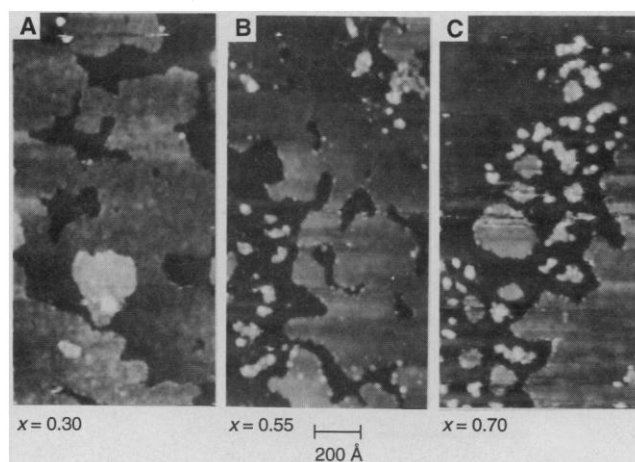


Fig. 3. Constant-current images of 880 Å by 1690 Å regions of (A) $\text{Ca}_{0.70}\text{Sr}_{0.30}\text{CuO}_2$, (B) $\text{Ca}_{0.45}\text{Sr}_{0.55}\text{CuO}_2$, and (C) $\text{Ca}_{0.30}\text{Sr}_{0.70}\text{CuO}_2$ film, respectively. The images were taken at a sample bias voltage of 2.0 V and a tunneling current of (A) 0.20 nA, (B) 0.10 nA, and (C) 0.10 nA.

The presence of the particles, depending on the Sr content of the films, suggests that the layer-by-layer growth process becomes progressively perturbed as the Sr content increases. One possible explanation is that the particles consist of Sr atoms expelled from the interior of the film because of their large ionic radius. In

related work (17) it was observed that SrCuO_2 films grown by atomic layer epitaxy exhibit a natural tendency for Sr deficiency. Feenstra *et al.* argued (17) that the Sr vacancies are incorporated to reduce the interfacial stress between the CuO_2 sheets and the intermediate alkaline earth metal layers (18). In our experi-

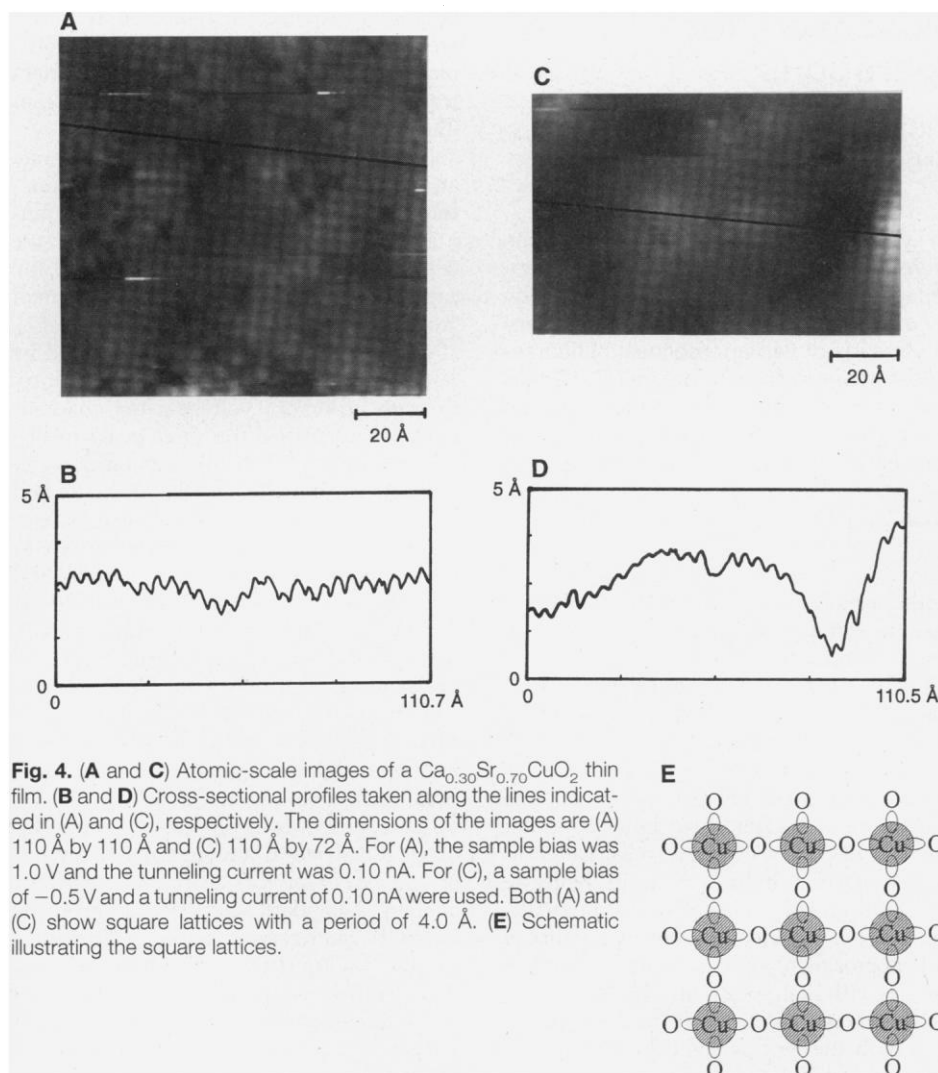


Fig. 4. (A and C) Atomic-scale images of a $\text{Ca}_{0.30}\text{Sr}_{0.70}\text{CuO}_2$ thin film. (B and D) Cross-sectional profiles taken along the lines indicated in (A) and (C), respectively. The dimensions of the images are (A) 110 Å by 110 Å and (C) 110 Å by 72 Å. For (A), the sample bias was 1.0 V and the tunneling current was 0.10 nA. For (C), a sample bias of -0.5 V and a tunneling current of 0.10 nA were used. Both (A) and (C) show square lattices with a period of 4.0 Å. (E) Schematic illustrating the square lattices.

ments, a stoichiometric (Sr+Ca):Cu mixture of 1:1 was supplied through the choice of target composition. In this case, Sr vacancy formation in the matrix of the infinite layer compound might lead to surface segregation of the expelled Sr atoms, as suggested by the trend of Fig. 3, A through C. This perturbed growth mechanism appears to have a profound impact on the doping mechanism of the films (19).

We have obtained atomic resolution STM images of the (Ca,Sr)CuO₂ films. Figure 4, A and C, show high-resolution STM images in the *ab* plane of a *c*-axis-oriented $\text{Ca}_{0.30}\text{Sr}_{0.70}\text{CuO}_2$ thin film on SrTiO₃(001). The STM image in Fig. 4A was taken with a sample bias voltage of 1.0 V. The image indicates an atomic square lattice of bright dots with randomly distributed point defects. Figure 4B shows the surface corrugation along the line indicated in Fig. 4A. The period of the dots is about 4.0 Å, which corresponds to the *a*-axis length of (Ca,Sr)CuO₂. For this

positive sample bias voltage, STM imaging senses the electronic structure of empty states. In the strongly correlated electronic system of the parent compound, electrons are tunneling into the Cu *d*¹⁰ band, which exists above the Fermi level (20). Thus, in this mode STM imaging appears to detect the Cu sites of the film. The density of the point defects varies from 7 to 14% with no apparent systematic dependence on the Sr/Ca ratio. The surfaces of the films with *x* = 0.55 and *x* = 0.70 contain particles presumably related to Sr atoms expelled from the parent compound matrix. The absence of such systematic dependence in the high-resolution images suggests that the point defects in Fig. 4A do not correspond to Sr or Ca. These defects are presumably due to Cu defects or to Cu¹⁺ ions in the presence of O vacancies.

On the other hand, the STM image of Fig. 4C, taken with a negative sample bias voltage of -0.5 V (occupied states), also shows a square atomic lattice with spacing

of 4 Å, similar to that in Fig. 4A. However, there are some obvious differences. The surface in Fig. 4A has considerable vertical undulations with an amplitude of about 3 Å. The corresponding cross-sectional profile (Fig. 4D) shows that lattice points can be seen even in the dark regions of Fig. 4C. These long-range undulations presumably arise from differences in the surface electronic structure.

The defect density in Fig. 4C is about 2%. This value is considerably smaller than that for the empty states. These observations suggest that the square lattice for the occupied states has a different origin than the empty state square lattice shown in Fig. 4A. Considering the strongly correlated electronic structure of this material, the oxygen 2*p* band is expected to contribute strongly to STM imaging below the Fermi level (20). However, in the ideal parent compound lattice, the oxygen atom configuration in the CuO₂ sheet does not correspond to a square lattice with spacing of 4.0 Å. Possibly, at the filled states, STM images reflect the hybrid orbitals consisting of Cu *d*⁹ and oxygen 2*p*, which also have a 4 Å square lattice periodicity, as shown in Fig. 4E. Further analysis, for example, the use of scanning tunneling spectroscopy to reflect the density of states, is needed to reveal the origin of the square lattices observed by STM imaging.

REFERENCES AND NOTES

1. T. Siegrist, S. M. Zahurak, D. W. Murphy, R. S. Roth, *Nature* **334**, 231 (1988).
2. M. D. Kirk *et al.*, *Science* **242**, 1673 (1988).
3. C. K. Shih, R. M. Feenstra, J. R. Kirtley, G. V. Chandrashekar, *Phys. Rev. B* **40**, 2682 (1989).
4. X. L. Wu, C. M. Lieber, D. S. Ginley, R. J. Baughman, *Appl. Phys. Lett.* **55**, 2129 (1989).
5. T. Hasegawa and K. Kitazawa, *Jpn. J. Appl. Phys.* **29**, L434 (1990).
6. X. L. Wu, Z. Zhang, Y. L. Wang, C. M. Lieber, *Science* **248**, 1211 (1990).
7. C. K. Shih, R. M. Feenstra, G. V. Chandrashekar, *Phys. Rev. B* **43**, 7913 (1991).
8. H. P. Lang, H. Häefke, G. Leemann, H.-J. Güntherodt, *Physica C* **194**, 81 (1992).
9. T. Hasegawa *et al.*, *J. Phys. Chem. Solids* **54**, 1351 (1993).
10. M. Nantoh *et al.*, *J. Appl. Phys.* **75**, 5227 (1994).
11. H. L. Edwards, J. T. Markert, A. L. de Lozanne, *Phys. Rev. Lett.* **69**, 2967 (1992).
12. ———, *J. Vac. Sci. Technol. B* **12**, 1886 (1994).
13. K. Koguchi, T. Matsumoto, T. Kawai, S. Kawai, *Jpn. J. Appl. Phys.* **33**, L514 (1994).
14. T. Matsumoto, H. Tanaka, K. Koguchi, T. Kawai, S. Kawai, *Surf. Sci.* **312**, 21 (1994).
15. X. Li, M. Kanai, T. Kawai, S. Kawai, *Jpn. J. Appl. Phys.* **31**, L217 (1992).
16. S. Gonda, H. Nagata, M. Kawasaki, M. Yoshimoto, H. Koinuma, *Physica C* **216**, 160 (1993).
17. R. Feenstra *et al.*, *ibid.* **224**, 300 (1994).
18. M. Takano, Y. Takeda, H. Okada, M. Miyamoto, T. Kusaka, *ibid.* **159**, 375 (1989).
19. R. Feenstra *et al.*, in preparation.
20. S. Uchida *et al.*, *Phys. Rev. B* **43**, 7942 (1991).
21. We thank R. Feenstra for helpful discussions and careful reading of the manuscript.

18 July 1994; accepted 26 October 1994